Received: 18 May 2023 | Revised: 21 June 2023 | Accepted: 5 July 2023

CAAI Transactions on Intelligence Technology

DOI: 10.1049/cit2.12267

ORIGINAL RESEARCH

D2LFS2Net: Multi-class skin lesion diagnosis using deep learning and variance-controlled Marine Predator optimisation: An application for precision medicine

Veena Dillshad[1] | Muhammad Attique Khan[1,2] | Muhammad Nazir[1] | Oumaima Saidani[3] | Nazik Alturki[3] | Seifedine Kadry[4]

[1]Department of Computer Science, HITEC University, Taxila, Pakistan

[2]Department of Computer Science and Mathematics, Lebanese American University, Beirut, Lebanon

[3]Department of Information Systems, College of Computer and Information Sciences, Princess Nourah bint Abdulrahman University, P.O. Box 84428, Riyadh 11671, Saudi Arabia

[4]Department of Electrical and Computer Engineering, Lebanese American University, Byblos, Lebanon

Correspondence

Seifedine Kadry.
Email: seifedine.kadry@lau.edu.lb

Funding information

Princess Nourah bint Abdulrahman University Researchers Supporting Project, Grant/Award Number: PNURSP2023R333

Abstract

In computer vision applications like surveillance and remote sensing, to mention a few, deep learning has had considerable success. Medical imaging still faces a number of difficulties, including intra-class similarity, a scarcity of training data, and poor contrast skin lesions, notably in the case of skin cancer. An optimisation-aided deep learning-based system is proposed for accurate multi-class skin lesion identification. The sequential procedures of the proposed system start with preprocessing and end with categorisation. The preprocessing step is where a hybrid contrast enhancement technique is initially proposed for lesion identification with healthy regions. Instead of flipping and rotating data, the outputs from the middle phases of the hybrid enhanced technique are employed for data augmentation in the next step. Next, two pre-trained deep learning models, MobileNetV2 and NasNet Mobile, are trained using deep transfer learning on the upgraded enriched dataset. Later, a dual-threshold serial approach is employed to obtain and combine the features of both models. The next step was the variance-controlled Marine Predator methodology, which the authors proposed as a superior optimisation method. The top features from the fused feature vector are classified using machine learning classifiers. The experimental strategy provided enhanced accuracy of 94.4% using the publicly available dataset HAM10000. Additionally, the proposed framework is evaluated compared to current approaches, with remarkable results.

KEYWORDS

artificial neural network, classification, computer vision, convolution, data fusion, feature extraction

1 | INTRODUCTION

Skin cancer is the abnormal proliferation of skin cells, and it typically affects people who have exposed their skin to the sun [1]. Melanomas, squamous, and basal cell carcinomas are the three most common types of skin cancer [2]. The seven main kinds of skin cancer include actinic keratoses and intraepithelial carcinoma/Bowen's disease (akiec), basal cell carcinoma (bcc), benign keratosis-like lesions (bkl), dermatofibroma (df), melanoma (mel), melanocytic nevi (nv), and vascular lesions (vasc) [3]. In the US, it is the most prevalent cancer. According to current projections, one in five Americans may get skin cancer at some point in their lives. Additionally, it is predicted that 9500 Americans will receive a skin cancer diagnosis every day. Over 3 million Americans are expected to be affected annually by other kinds of skin cancer, such as basal cell carcinoma (BCC) and squamous cell carcinoma (SCC). Seven thousand six hundred fifty people will pass away from the disease in 2022, when it is anticipated that 99,780 new cases of invasive melanoma and 97,920 cases of stage zero melanoma will be

discovered in the country. Research shows that women are more likely than men to develop skin cancer before age 50. Men continue to see an increasing increase in incidence after that (www.cancer.org/research/cancer-facts-statistics/all-cancer-facts-figures/cancer-facts-figures-2022.html). For both sexes, an invasive melanoma is the seventh most common malignancy to be discovered. In the United States, melanoma rates have rapidly increased over the past 30 years, doubling from 1982 to 2011. Men are 1 in 27 more likely than women to develop melanoma in their lifetime, and women are 1 in 40 more likely [4].

Only around 60% of cutaneous melanoma diagnoses are accurately made by the unaided eye. One of the most popular conventional clinical techniques for locating and identifying skin lesions is dermoscopy [5]. It is a technique for skin surface microscopic inspection. It is additionally known as 'epiluminoscopy'. Dermoscopy is a useful method for melanoma diagnosis, and when utilised by specialists, it has increased diagnostic accuracy. The accuracy of diagnosis is significantly impacted by dermatologists' experience [6]. Traditional CAD methods which are usually employed for diagnosis include the ABCD rule [7], 3-point checklist [8], 7-point checklist [9], Menzies score [10], and CASH (Colour, Architecture, Symmetry, and Homogeneity) Algorithm [11].

It has been demonstrated that applying computational intelligence techniques can help dermatologists and general practitioners analyse data more rapidly and increase the accuracy of their diagnoses [12–14]. Preprocessing, segmentation, feature extraction, selection, and classification make up a typical computer-aided diagnostic (CAD) system for identifying and classifying skin lesions [15]. Many researchers have contributed to developing automated diagnostic tools for effective skin lesion separation and classification, focusing on various stages of the CAD system and incorporating various computing technologies [16, 17]. With the advancement of research and development in automated diagnostic tools, new challenges must be addressed to increase the utility of these CAD systems [18]. Despite the higher detection rate with dermoscopy, its accuracy highly depends on varying factors, that is, the experience and training of dermatologists. To aid dermatologists, numerous computer-aided techniques were presented in the literature. In addition, researchers introduced image processing techniques to analyse the lesion images and declare whether the image is of normal skin or cancerous skin [19]. All CAD systems consist of key steps involving image acquisition, border detection to separate lesion from healthy skin, feature extraction, and feature classification [20]. Most of the traditional CAD systems used histogram thresholding, global thresholding, and morphological operators for border detection. The features mostly used for classification are colour, texture, asymmetry, border irregularity, diameter, and geometry-based features [21, 22].

All these traditional CAD systems depend on features that are manually extracted from an input image. These calculated features are inadequate to recognise complicated or understated diseases effectively and are not robust against variations. Compared to the traditional approach towards feature extraction in machine learning (ML), deep learning (DL) methods intend to learn feature hierarchies [23]. Feature hierarchies are such that the arrangement makes features from a higher level of lower-level features. This autonomous feature learning at different generalisation levels helps the system understand intricate functions that map the input directly to the output and does not rely entirely on human-crafted features [24]. In medical imaging, deep learning is employed for several tasks, such as segmentation and classification. For these tasks, the performance of deep learning methods is exceptional. However, skin lesion classification in medical imaging is a complex problem in which more than six classes have been included [23]. The intra-class similarity of each class is high, and the number of images of each class is highly imbalanced. For a deep learning model, more images are required for better training; therefore, in this work, we consider the following challenges: (i) low contrast lesions; (ii) imbalanced dataset; (iii) high computational time after features fusion. We proposed a new automated framework based on deep learning and an optimisation algorithm to resolve these challenges. Major contributions of this work are as follows:

- Proposed a hybrid approach for lesion contrast enhancement. The middle step outputs are employed as a data augmentation instead of flip and rotation.
- The augmented enhanced dataset is employed for the training of fine-tuned models instead of training models on the original dataset using deep transfer learning.
- Proposed a serial-based dual threshold fusion approach.
- Developed a better variances-controlled MPA optimisation technique to choose the optimal features.

The rest of the manuscript is organised in the following order. First, related work that consists of the summary of existing techniques is presented in Section 2. Then, the proposed methodology, including the hybrid contrast stretching technique, augmentation of the original dataset, deep learning models fine-tuning, and proposed features selection technique, are discussed in Section 3. Next, the results are discussed in Section 4. Finally, concludes the manuscript under Section 5.

2 | RELATED WORK

Recently, researchers have made many contributions to fully automate the diagnosis process and increase the reliability of computer-aided skin lesion diagnostic systems [25]. Much research has been conducted on the binary classification of the most lethal type of skin lesion, melanoma [26]. However, there are six other skin lesions, many of which are just as dangerous as melanoma if not detected early. As a result, early detection and accurate classification of multi-class skin lesions are critical. The high similarity between lesions of different classes and the drastic differences among skin lesions of the same class makes multi-class skin lesions classification one of the most difficult challenges [27]. All stages of a CAD system for multi-class skin

lesion diagnosis, including preprocessing, segmentation, feature extraction, best feature selection, and classification, are active research areas. Deep learning-based automatic skin lesion diagnostic systems are thoroughly studied in [28, 29], and [30]. Farhat et al. [31] presented an improved method for the multi-class categorisation of skin lesions. They extracted deep features using transfer learning, and then obtained features were optimised by hybrid whale optimisation and Entropy Mutual Information (EMI) techniques. After acquiring optimised features, fusion is performed using reformed canonical correlation-based approach, and at last extreme learning machine-based classification is done. The presented approach is tested on HAM10000 and ISIC2018 datasets and obtained 93.4% and 94.36% accuracy, respectively. In ref. [32], authors preprocessed the acquired images to remove artefacts and improve quality, then segmented the region of interest using Geodesic Active Contours (GAC). For feature extraction, two methods are used: Score features are extracted through CNN (ResNet-18 is used for transfer learning) and texture features are extracted using GLCM and HOG methods. Finally, classification is done using an SVM classifier.

Authors in ref. [33] designed and developed a deep convolutional neural network with many layers and filter sizes but used fewer filters and parameters to increase efficiency and performance. The datasets used to evaluate the presented work are ISIC2017, ISIC2018, and ISIC2019. The primary objective of the presented work was to minimise preprocessing operations. In ref. [34], Khan et al. presented a DL-based skin cancer recognition system. This work focused on preprocessing phase and later determining the most discriminant feature. Both these factors contributed to the reduction of computational time and complexity. ISBI2016 and ISBI2017 datasets were used to perform tests. Similarly, another work in ref. [35] utilised refinement and augmentation networks. In ref. [36], Hasan et al. focused on the importance of preprocessing step. First, the images were enhanced using the Gaussian Blur approach, and later edges were detected to achieve a specific border of artefacts. After that, the image mask was generated and restored without artefacts in the database. To combat the lesion contrast problem, researchers in ref. [37] presented a novel preprocessing technique that was executed on a black-and-white image, which enhanced the contrast by lowering variations in light intensity of the lesion area. In ref. [38], preprocessing uses a top hat filter and inpainting technique. In ref. [39], authors focused on addressing motion-blurred images by exploring genetic algorithms for enhancing image quality. In ref. [40], Khan et al. gave automated multi-class skin lesion segmentation and classification, consuming deep features. This approach first includes input image enhancement using LCcHIV.

Extracting features and selecting the optimal ones is important in creating an accurate predictive model. In ref. [34], Khan et al. implemented a new DL model that was based on the selection of best features named the iteration-controlled Newton-Raphson (IcNR) technique. In ref. [41], the authors presented a new skin lesion classification system using a deep neural network (DCNN) based on transfer learning for feature extraction and kurtosis-controlled principal component (KcPCA) based on ideal feature selection. Experiments utilised datasets HAM10000, ISBI 2017, and ISBI2016 and acquired an accuracy of 89.8%, 95.60%, and 90.20%, respectively. In ref. [42], researchers presented an efficient approach combining information from DL and handcrafted features, showing improved accuracy on the selected datasets. First, in ref. [37], handcrafted features such as shape, texture, local, and global are extracted. After that, features were fused, and finally, optimum features were selected based on a genetic algorithm. In ref. [43], the inception CNN model extracted deep features on two basic output layers. After that, the decision-controlled parallel fusion method is employed for feature fusion. Finally, the best features are selected using a window distance-controlled entropy approach. There are several other studies are also presented that used the pre-trained models for the classification [23, 44, 45]. A few researchers introduced some traditional techniques for the desired results [46].

In all the above techniques, the researchers did not focus on the contrast enhancement step, and the maximum ignored the data augmentation process. The data augmentation step usually performed using flip and rotation based operations; however, these operations are not useful and sometimes degrade the training accuracy that later decreased the classification accuracy. Moreover, they considered the feature selection process that improved the accuracy and reduced the time. In this work, we proposed a new method based on contrast-enhanced deep learning features and optimal feature selection for accurate multi-class skin lesion classification.

3 | PROPOSED METHODOLOGY

This section provides a thorough mathematical and theoretical explanation of the proposed multi-class skin lesion categorisation framework. As seen in Figure 1, the suggested framework includes several crucial processes, from data augmentation to classification. The first phase involves doing data augmentation using various contrast-enhancing methods. The next phase involved using and fine-tuning two pre-trained deep learning architectures per the selected dataset's characteristics. Deep transfer learning was used to train the refined models without a freezing layer. Both trained models provide two feature vectors combined using an enhanced serial-based method. Later, a better optimisation is chosen to pick the best features and shorten the calculation time. Machine learning classifiers classify the best features at the end. Subsections that follow each stage are described in further detail.

3.1 | Datasets

This study employs the HAM10000 (Human Against Machine) dataset to assess the proposed system. The Department of Dermatology at the Medical University of Vienna, Austria, and Cliff Rosendahl's skin cancer clinic in Queensland, Australia, respectively, provided the 10,015 photographs that make up

this dataset, which was compiled over a 20-year period [47]. Early datasets typically had issues with either small size or a lack of variety in dermoscopic images. 6705 photos of melanocytic nevi, 1113 images of melanoma, 1099 images of benign keratoses, 514 images of basal cell carcinoma, 327 photographs of actinic keratoses, 142 images of vascular, and 115 images of dermatofibroma lesions are included in this collection. The sample photos of each lesion type in this dataset are shown in Figure 2.

3.2 | Data augmentation using hybrid contrast enhancement

We proposed a hybrid contrast enhancement technique to improve lesion regions in this work. The proposed hybrid technique is based on three middle steps: local contrast improvement, laplacian filter, and global contrast improvement. In the end, the fusion is performed to combine middle images. This process is defined under Algorithm 1.

Algorithm 1 Proposed algorithm of hybrid contrast enhancement and augmentation.

Input Image $\leftarrow \varphi(x,y)$
Output Image $\leftarrow \tilde{\varphi}(x,y)$
Step 1: Initialize structuring element
$se \leftarrow \mu$
$\mu = Mean(\varphi(x,y))$
Step 2: **for** i=1 to N Images
$\varphi_1(x,y) \leftarrow LC(\varphi(x,y), se)$
$LC = E(\varphi^2) - [E(\varphi)]^2$
$\varphi_2(x,y) \leftarrow Lp(\varphi(x,y))$
$\varphi_3(x,y) \leftarrow Gl(\varphi(x,y), se)$
$Gl = \lambda_1(x,y) - \lambda_2(x,y)$
$\lambda_1(x,y) = \varphi(x,y) + (\varphi(x,y) \circ se)$
$\lambda_2(x,y) = (\varphi(x,y) \cdot se) - \varphi(x,y)$
Step 3: $\tilde{\varphi}(x,y) \leftarrow Fused(\varphi_1, \varphi_2, \varphi_3)$
Step 4: Write Image $\varphi_1(x,y)$
Step 5: Write Image $\varphi_2(x,y)$
Step 6: Write Image $\tilde{\varphi}(x,y)$
End **for**

In the above steps, se denotes the structuring element, μ denotes the mean value of an original image, $\varphi_1(x, y)$ denotes the local contrast-enhanced image, as shown in Figure 3b, $\varphi_2(x, y)$ denotes the local laplacian filtered image (seen in Figure 3c), and $\tilde{\varphi}(x,y)$ is a final fused image (seen in Figure 3d), respectively. Each middle-processed image is also saved for the data augmentation process. The numbers of images after the data augmentation are presented in Table 1.

3.3 | Pre-trained deep learning models

Let, $I : \varpi \rightarrow F^{d\ x\ \eta_{TS}}$ represent input RGB image sequence of skin lesion images. The size of each image in the sequence is 224 × 224 pixels. Let ϖ^{+}be the subset such that $\varpi^{+} \subset \eta_{TS}$. In addition to this $\acute{L}_T \rightarrow F^{O_c x\ \eta_{TS}}$, signifies the equivalent label matrix for each input image sequence, where η_{TS} denotes the number of training images, d represents dimension, and O_c represents the number of classes. All network layers are explained individually in the proceeding sections.

The convolutional layer is the elementary module of CNN architecture. This block utilises multiple filters with variable weights and biases to get the most prominent features and characterise them as an output feature map. If we take $\mathfrak{F}^{i-1}$ as an input feature map, the output from layer i−1, C_k^i as convolutional kernel and β_k^i as the bias at ith layer than for the kth output feature map $\mathfrak{F}_k^i$ at the ith a layer is convolved with kth kernel of ith layer, and finally, bias is added. This same process is repeated for each convolutional layer of the proposed framework. The output of this layer is passed through batch normalisation $\mathfrak{B}(\bullet)$. Nonlinear activation function $\mathfrak{r}(\bullet)$ follows batch normalisation. The process of a convolutional layer is represented in Equation (1).

$$\mathfrak{F}_k^i = \mathfrak{r}\left(\mathfrak{B}\left(\sum_{r=1}^{m} \mathfrak{F}_r^{i-1} * C_{k_r}^i + \beta_k^i\right)\right) \tag{1}$$

Another layer named ReLu is used as an activation function $\mathfrak{r}(\bullet)$, stacked with each convolutional layer. In this activation function, values less than zero are swapped by zero, and values greater or equal to zero are kept unchanged, as defined in Equation (2).

$$\mathfrak{r}\left(\mathfrak{F}_k^i\right) = \max\left(0, \mathfrak{F}_k^i\right) \tag{2}$$

Batch normalisation $\mathfrak{B}(\bullet)$ layers are employed in CNN after every convolutional layer and follow the first and second fully connected layers also. This layer is used to moderate stability and increase the speed of the training process. This layer normalises feature maps, output from the convolutional layer by deducting the mean (M_Ψ) of mini-batch Ψ. The value of Ψ can be from, $\Psi \subset \{1, 2, 3, \ldots, 32\}$ and dividing by the standard deviation SD_Ψ of a batch, as described in Equation (3).

$$\mathfrak{B}\left(\mathfrak{F}_k^i\right) = \mathfrak{F}_k^i - M_\Psi \ / \ \sqrt{SD_\Psi^2 + \varsigma} \tag{3}$$

Where, $\varsigma = e^{-0.5}$ is a constant which aims to evade complex values.

Another important layer is named a pooling layer. In this layer, the dimensions of the feature map are reduced by the down-sampling. This decreases the number of succeeding learnable parameters. Features are extracted in the fully connected layer. This layer reduced the feature map into 1D (one-dimensional) feature vector denoted by $\mathfrak{F}^{i-1}$. Mathematically, this layer is defined as follows:

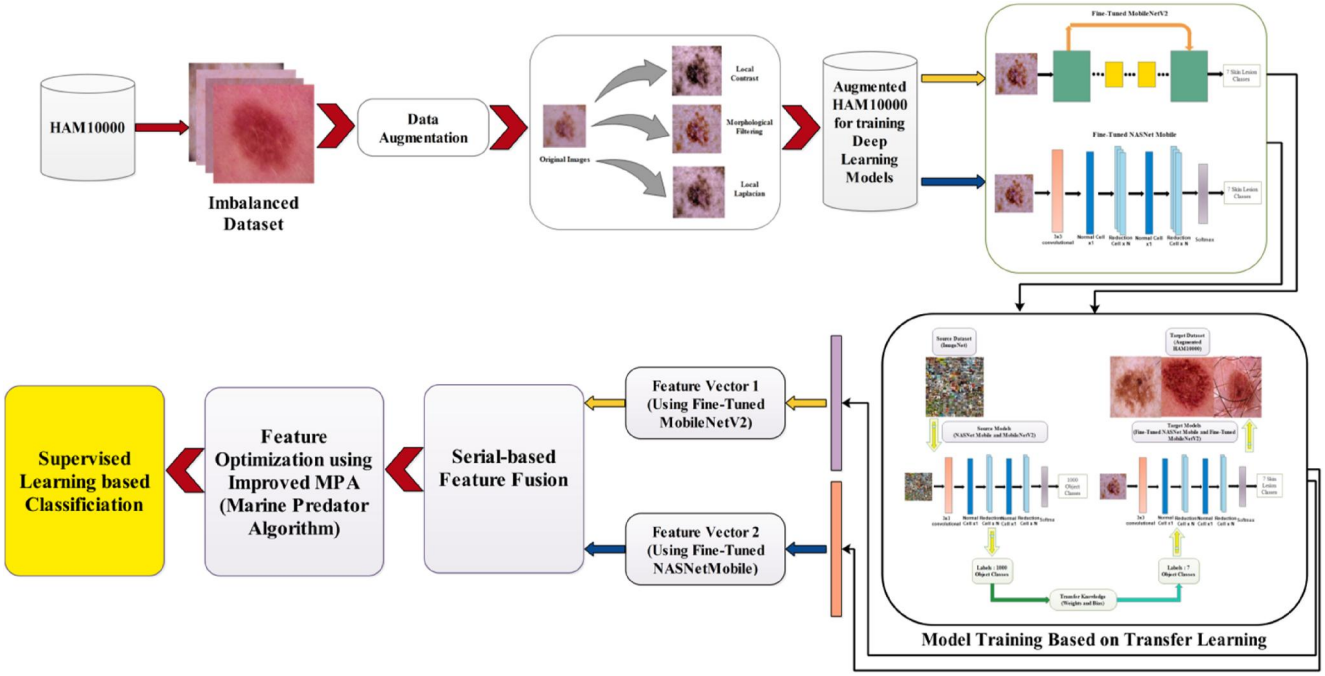

FIGURE 1 Proposed framework for multi-class skin lesion classification.

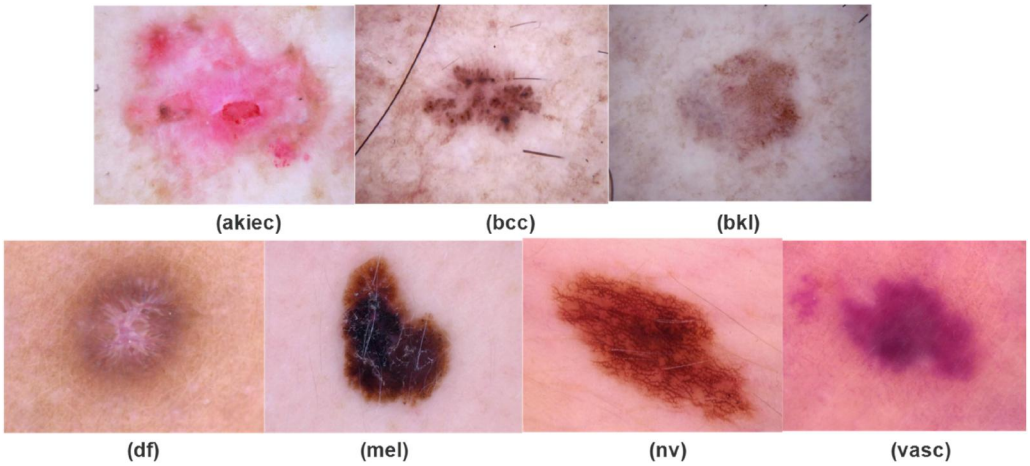

FIGURE 2 Sample images of skin lesion types collected from the HAM10000 dataset.

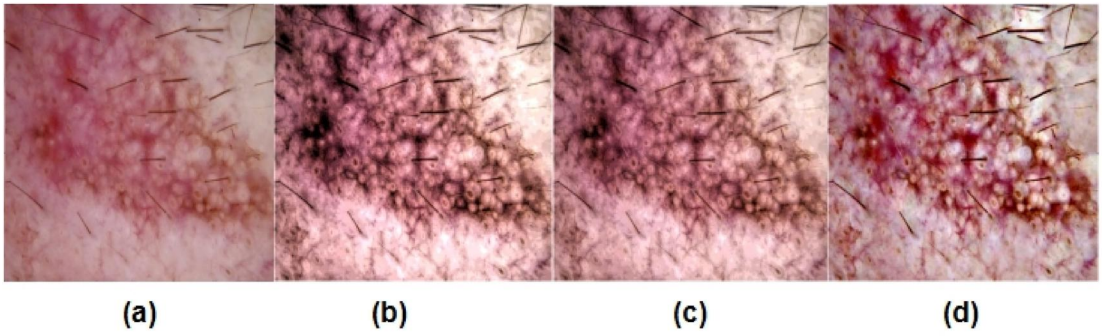

FIGURE 3 Sample images of lesion enhancement using the proposed hybrid approach. (a) Original image, (b) local contrast, (c) local laplacian, (d) final hybrid technique image.

TABLE 1 Description of the original HAM10000 dataset and augmented HAM10000 dataset.

Class/dataset	HAM10000	Augmented HAM10000
Akiec	327	4291
Bcc	514	4247
Bkl	1099	4247
Df	115	4357
Mel	1113	4308
Nv	6705	4348
Vasc	142	4215

$$FC_L^i = \mathfrak{Y}\left(\mathfrak{B}\left(\sum_{r=1}^{m} \mathfrak{F}_r^{i-1} * C_{k_r}^i + \beta_k^r\right)\right) \quad (4)$$

In this framework, we have used two fine-tuned deep learning models MobileNet V2 and NASNet Mobile. MobileNetV2 [48], a faster and more accurate version of its predecessor MobilenetV1, is selected for this framework. It is a lightweight model that can be trained on devices with low computational power. So, it is beneficial in resource-constrained environments. In MobileNetV2, there are two types of blocks. One is a residual block with a stride of 1, and the other is a block for reasoning with a stride of 2. There are three more layers on each block. ReLU6 is used in 1×1 convolution as the initial layer. The last layer is gain 1×1 convolution without non-linearity, that is, without ReLU6, while the second layer is depth-wise convolution. Because MobileNetV2 has fewer channels than MobileNetV1, it is quicker than MobileNetV1. MobileNetV2 is more precise when there is a residual connection.

The NASNet (Neural Architecture Search) [49], the second model used in the proposed framework, automates the process of network architecture selection. It searches for the best algorithm that achieves maximum performance on a given task. First, Controller RNN predicts the Normal and Reduction blocks. These blocks are not predefined in NASNet. For each block, RNN selects two hidden states from a set of hidden states created in preceding iterations, then selects an operator to be performed on each of these states from a set of operators. Finally, it must select the method to combine the outputs of these operators. The result of this process is retained as another hidden state which will be utilised in the subsequent blocks. NASNet aims to discover the best combinations from a set of operations with the help of controller RNN to construct a block with the best performance instead of designing the block using handcrafted decisions.

In this framework, these two models are trained on the augmented dataset using a deep transfer learning approach. First, through deep TL, weights of original models are utilised and mapped on the fine-tuned model. Then the fine-tuned model is trained from scratch instead of freezing some layers. Visually, the process of deep TL is shown in Figure 4. For both models, all parameters have been trained such as 3.5 M (million) for MobileNet V2 and 5.3 M for NasNetMobile. In this figure, it is illustrated that the original deep models were trained on the ImageNet dataset. After that, the fine-tuning process is performed, and transfers the knowledge. Then, fine-tuned models are trained on the augmented HAM10000 dataset and obtained new models with seven classes in the output layer.

3.4 | Features extraction

After training using deep TL, two models, such as Modified MobilenetV2 and Modified NASNet, are produced. The Global Average Pooling (GAP) layer is chosen and activated for MobileNetV2 that has been tuned. As an activation function, the entropy loss function is used. The 1280 features are extracted for each image on this layer. Similar to this, the Global Average pooling (GAP) layer is chosen and activated for fine-tuned NASNet Mobile. As an activation function, the entropy loss function generated 1056 features for each image. We employed a number of hyperparameters throughout the training phase, including learning rate of 0.0001, mini-batch size of 8, stochastic gradient descent as the optimisation approach, and momentum of 0.7. The following step involves fusing the extracted characteristics using a single-level threshold function.

3.5 | Proposed features fusion

Features fusion is the process of combining multiple feature vectors into a single feature vector. The main purpose of this step is to improve the information about an object or disease based on multi-characteristics [44]. We proposed a dual threshold function-based serial approach for fusing both feature vectors in this work. The proposed approach is based on two serial steps. In the first step, features are horizontally concatenated, and in the second step, the threshold function is employed based on the median value for final fusion. Mathematically, this process is defined as follows:

Consider we have two obtained feature vectors F_1 and F_2 having dimension $N \times 1280$ and $N \times 1056$, respectively. Let, F_3 is the initial concatenated feature vector of dimension $N \times K$ that is obtained as follows:

$$F_3 = \begin{pmatrix} F_1 \\ F_2 \end{pmatrix}_{(N\times 1280 + N\times 1050)} \quad (5)$$

The median value Md is computed from this vector and defined as a threshold function. The value of Md is computed as: $\text{Md} = \frac{\text{Total features of F3}}{n}$. Through the threshold function, some features that do not meet the criteria are reduced.

$$T = \begin{cases} F_{fs} & \text{for} \quad F_3 \geq \text{Md} \\ F_{fs1} & \text{for} \quad F3 < \text{Md} \end{cases} \quad (6)$$

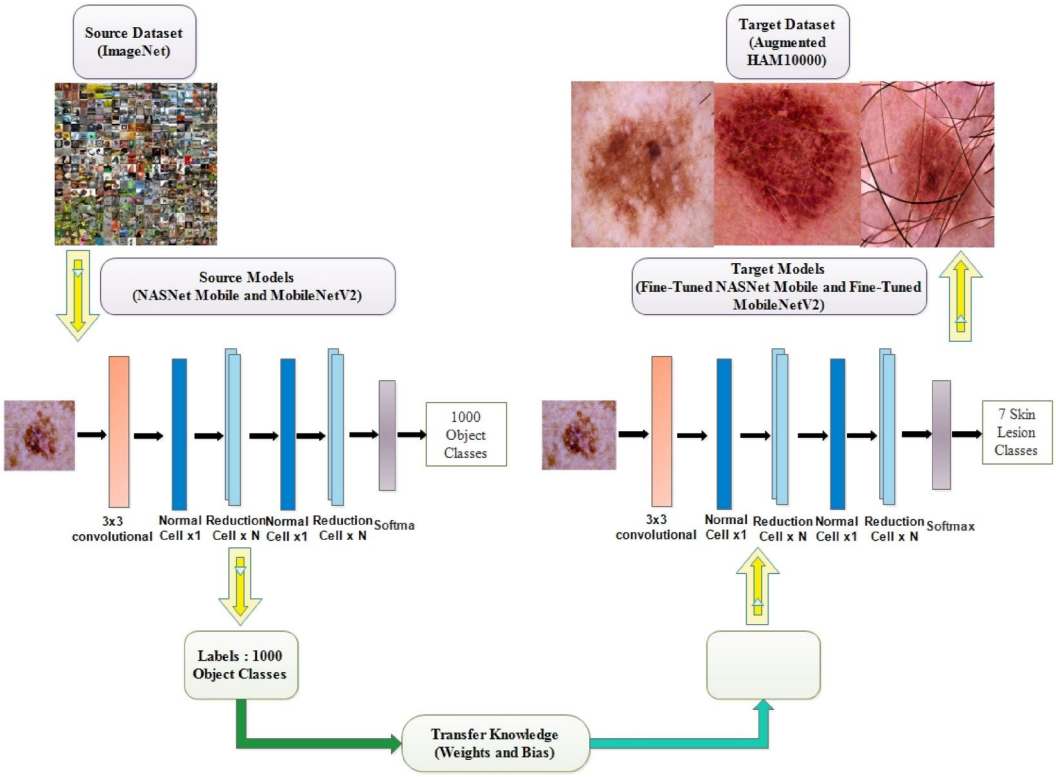

FIGURE 4 Process of deep TL for training a pre-trained model for skin lesion classification.

$$T1 = \begin{cases} F_{fs2} & \text{for} \quad F_{fs1} \geq \mathrm{Md}(F_{fs1}) \\ \text{Else, ignore values} \end{cases} \tag{7}$$

$$\tilde{F} = \begin{pmatrix} F_{fs} \\ F_{fs2} \end{pmatrix}_{(N\times K1+N\times K2)} \tag{8}$$

Where, $\tilde{F}$ denotes the fused feature vector of dimension $N \times 1590$. This process improves the classification performance, but there include some redundant features. Therefore, it is essential to reduce those irrelevant features through an optimisation approach.

3.6 | Proposed optimisation algorithm

In this work, we proposed a variance-controlled Marine Predators Algorithm (VcMPA) algorithm for the best features selection. MPA is inspired by the Levy and Brownian movement pattern in ocean predators. In the original MPA, the solution is distributed homogeneously over the search space and mathematically defined as follows:

$$X_o = X_{\min} + \mathrm{rand}\,(X_{\max} - X_{\min}) \tag{9}$$

Where, rand is a uniform random vector in the limit [0, 1] and $X_{\max}$ and $X_{\min}$ are lower and upper constraints for variables. According to the theory of 'survival of the fittest', the best predators are the fittest for hunting. So, in MPA, the fittest solution is given the rank of best predator and is used to build a matrix Elite E_i as follows:

$$\mathsf{E}_i = \begin{matrix} X^l_{1,1} & X^l_{1,2}\ldots\ldots & X^l_{1,d} \\ X^l_{2,1} & X^l_{2,2}\ldots\ldots & X^l_{2,d} \\ . & . & . \\ . & . & . \\ \dot{X^l}_{n,1} & \dot{X^l}_{n,2}\ldots\ldots & \dot{X^l}_{n,d} \end{matrix} \tag{10}$$

Where, X^l is the best predator, which is duplicated n times to create this matrix. The n is the number of search agents, which are both predators as well as prey, and d denotes the dimension of a matrix. After every iteration in the optimisation process, this matric is updated to replace the best predator with the better one. The initial matrix named prey is created through the below equation and called the best fittest predator that makes the Elite matrix.

$$\mathsf{P}_i = \begin{matrix} X_{1,1} & X_{1,2}\ldots\ldots & X_{1,d} \\ X_{2,1} & X_{2,2}\ldots\ldots & X_{2,d} \\ . & . & . \\ . & . & . \\ . & . & . \\ X_{n,1} & X_{n,2} & X_{n,d} \end{matrix} \tag{11}$$

Where, $X_{i,j}$ is the jth dimension of ith prey and $\mathcal{P}_i$ is the best fittest predator Elite matrix. By analysing the velocity ratio of predators and prey, MPA divides the optimisation process into three phases: High-velocity ratio, unit velocity ratio, and low-velocity ratio. For all phases, the number of iterations is fixed. These specifications are based on the natural movements of prey and predators. In the starting iterations, prey is moving at a higher speed than predators. In this phase exploration is important, so the most appropriate strategy for a predator is not to move at all. This rule is mathematically presented as follows:

While iter < $\frac{1}{3}$ maxIter

$$\text{stepsize}_i = \check{R}_B \otimes \left(\hat{\mathcal{E}}_i - \check{R}_B \otimes \mathcal{P}_i\right) \quad i = 1 \ldots n \tag{12}$$

$$\mathcal{P}_i = \mathcal{P}_i + \text{p.r} \otimes \text{stepsize}_i \tag{13}$$

In this formulation, $\check{R}_B$ is a vector of numbers representing Brownian motion, $\otimes$ represents entry-wise multiplication, ($\hat{\mathcal{E}}_i$) represents the top predator, $\mathcal{P}_i$ represents the prey, p is a constant value that is 0.5, and r is uniform random numbers in [0, 1]. The variable iter is the current iteration, and maxIter denotes the maximum iteration. In the second phase, prey and predator move at identical speeds. This stage occurs at the intermediate iterations, so exploration and exploitation are important here. Due to this reason, one part of the population $\left(\frac{n}{2}\right)$ is responsible for exploitation; the remaining part is specified for exploration. In MPA, it is considered for this phase that prey follows Lévy motion, and the predator is moving in Brownian motion. Rules for this phase are shown mathematically as follows:

$$\text{While } \frac{1}{3} \text{ maxIter} < \text{iter} < \frac{2}{3} \text{ maxIter} \tag{14}$$

$$\text{stepsize}_i = \check{R}_L \otimes \left(\hat{\mathcal{E}}_i - \check{R}_L \otimes \mathcal{P}_i\right) \quad i = 1 \ldots n/2 \tag{15}$$

$$\mathcal{P}_i = \mathcal{P}_i + \text{p.r} \otimes \text{stepsize}_i \tag{16}$$

Where, $\check{R}_L$ is a vector consisting of random numbers founded on Lévy distribution, representing Lévy movement. $\check{R}_L$ and $\mathcal{P}_i$ are multiplied to mimic the Lévy movement of prey, and step size is added to the prey's position to represent the prey's movement. This section helps in exploitation. For the remaining half of the population, rules are defined as follows:

$$\text{stepsize}_i = \check{R}_B \otimes \left(\check{R}_B \otimes \hat{\mathcal{E}}_i - \mathcal{P}_i\right) \quad i = 1 \ldots n/2 \tag{17}$$

$$\mathcal{P}_i = \hat{\mathcal{E}}_i + p.CF \otimes \text{stepsize}_i \tag{18}$$

Where, CF is the controlling factor that controls step size for a predator. $\check{R}_B$ and $\hat{\mathcal{E}}_i$ are multiplied to mimic the predator's movement in Brownian fashion, and prey revises its position based on this Brownian movement of predators. In the last stage, a predator moves faster than the prey. This is the last stage of iterations in the optimisation process. It is linked with high-level exploitation. The top suggested approach for predators in this phase is Lévy, which is defined as follows:

While iter > $\frac{2}{3}$ maxIter

$$\text{stepsize}_i = \check{R}_L \otimes \left(\check{R}_L \otimes \hat{\mathcal{E}}_i - \mathcal{P}_i\right) \quad i = 1 \ldots n \tag{19}$$

$$\mathcal{P}_i = \hat{\mathcal{E}}_i + \text{p.CF} \otimes \text{stepsize}_i \tag{20}$$

Multiplication of $\check{R}_L$ and $\hat{\mathcal{E}}_i$ mimics the Lévy movement of the predator, and adding the step size to the top predator matrix represents the predator's movement that ultimately helps the target to update its position. Environmental factors that affect the behaviour of predators is eddy formation or Fish Aggregating Devices (FAD). They act as local optima in the optimisation process. This effect is represented as follows:

$$\mathcal{P}_i = \begin{cases} \mathcal{P}_i + \text{CF}\left[X_{\min} + \check{R}_L \otimes (X_{\max} - X_{\min})\right] \otimes U & \text{If } r < \text{FADs} \\ \mathcal{P}_i + [\text{FADs}\,(1-r) + r](\mathcal{P}_{x1} - \mathcal{P}_{x2}) & \text{If } r > \text{FADs} \end{cases} \tag{21}$$

Where, the value of FAD is 0.4, U is a binary vector. Arrays of this vector comprise of zeros and ones. It is initialised randomly in [0, 1] and then shifted its arrays to either 0 or 1, depending on the following rule: it shifts to 0 if array <0.4 and to one if it is >0.4. The r is a uniform random number in between [0, 1]. $X_{\max}$, $X_{\min}$ are the vectors containing the lower and upper bound of dimensions. The $\mathcal{P}_{x1}$, $\mathcal{P}_{x2}$ are any two targets from prey matrix. After revising prey and applying FAD effect, the matrix is assessed for the fittest solution to renew $\hat{\mathcal{E}}_i$. The fittest solutions are later checked through variance based activation function as follows:

$$\begin{cases} \mathcal{P}_i(vr) \quad if \quad \hat{\mathcal{E}}_i \geq \text{var} \\ \text{Ignore, Elsewhere} \end{cases} \tag{22}$$

$$\text{var} = \sum \frac{\left(\hat{\mathcal{E}}_i - \overline{\hat{\mathcal{E}}}\right)}{n-1} \tag{23}$$

The resultant feature vector $\mathcal{P}_i(vr)$ is passed to the fitness function for fitness calculation and compared with prior solutions. If it is the fittest, the current solution replaces the previous solution. This process continues for the maximum number of iterations, as 200 iterations are selected in this work.

4 | RESULTS AND DISCUSSION

The outcomes of the suggested framework are provided in this section. The suggested system has been tested using the enhanced HAM10000 dermoscopic dataset. The results of the training and testing have been chosen by the 50:50 strategy. The testing results are used with the 10-fold cross-validation method. For the classification outcomes, several classifiers have been used, including Linear SVM. Medium Gaussian

SVM, Coarse Gaussian SVM, Cosine KNN, Cubic KNN, and Weighted KNN are among the SVM algorithms. Accuracy, sensitivity, precision, F-1 Score, and classification time are performance metrics that are computed for each classifier. MATLAB2022b is used to simulate the full structure on a computer with 16 GB of RAM and an 8 GB graphics card.

4.1 | Numerical results

In this experiment, classification is carried out using fine-tuned MobileNetV2 model characteristics. Table 2 provides a summary of the experiment's findings. Ten distinct classifiers' classification results are shown in this table. For Cubic SVM, the highest accuracy possible was 85.7%. Additionally calculated are the sensitivity, precision, and F1 Score, with values of 85.7%, 85.7%, and 85.75%, respectively. The accuracy rates for the other classifiers included in this table were 83.2%, 84.9%, 84.8%, 81.2%, 83.4%, 81.4%, 81.3%, 80.6%, and 82.8%, respectively. It should be mentioned that the quadratic SVM attained the second-best accuracy of 84.9% based on these accuracy figures. Additionally, the computational time for each classifier is mentioned, with the Fine KNN classifier taking the least amount of time (133.22 s).

The refined NASNet Mobile model's deep features classification accuracy is displayed in Table 3. As with optimised MobileNet-V2, an enhanced HAM10000 dataset is used for training. The quadratic SVM classifier had a maximum accuracy of 93.2% in this table. Additionally computed values for sensitivity, accuracy, and F1 Score are 93.08%, 93.05%, and 93.16%, respectively. When comparing this experiment's accuracy and other computed metrics to experiment 1, it was found that the Nasnet Mobile features increased accuracy by about 8%. It is also stated that NasNet Mobile's computing time is longer than that of MobileNet-V2, which is also acknowledged. Fusion is carried out in the final phase utilising the suggested dual threshold serial technique.

The proposed dual threshold serial approach-based fusion is carried out in this experiment, and the results are shown in Table. In this table, the Quadratic SVM classifier's maximum accuracy was 93.6%. Additionally computed values for sensitivity, accuracy, and F1 Score are 93.62%, 93.68%, and 93.65%. An additional confirmation of the sensitivity rate can be found in the confusion matrix shown in Figure 5. The accuracy of the bkl and melanoma classes is shown in this image to be below 90%, while the accuracy of the vasc class is shown to be 99.1%. Overall, compared to experiments 1 and 2, the hypothesised fusion mechanism is more accurate. Additionally, the sensitivity, accuracy, and F1-Score values have all increased. Each implemented classifier's computational time is given as well, with a minimum reported duration of 421.6 (sec). This experiment took longer to complete than the first two trials, which is a disadvantage of fusion.

The final experiment uses a proposed Variances controlled MPA optimisation algorithm to optimise the fused features. The outcomes of this experiment are presented in Table 4. The Cubic SVM classifier had the highest overall accuracy of 94.4% of the 10 different classifiers' results. Additionally calculated, the values for sensitivity, precision, and F1 Score are 94.4%, 94.4%, and 94.4%, respectively. Figure 6 also shows the Cubic SVM's confusion matrix, which can be used to confirm the suggested sensitivity rate. Additionally, the Fine KNN classifier's minimum computing time for this experiment is 183.3 s, while the maximum reported time is 378.6 s. When the results of this experiment are compared to Tables 2, 3 and 5, it is obvious that the accuracy has increased thanks to the

TABLE 2 Classification results of fine-tuned MobileNetV2 features using augmented HAM10000 dataset.

	Performance measures				
Classifiers	**Accuracy (%)**	**Sensitivity (%)**	**Precision (%)**	**F1-score (%)**	**Time (sec)**
Linear SVM	83.2	83.13	83.27	83.19	208.27
Quadratic SVM	84.9	84.92	84.971	84.94	262.91
Medium Gaussian SVM	84.8	84.8	71.11	77.35	384.06
Coarse Gaussian SVM	81.2	81.24	81.64	81.44	357.71
Fine KNN	83.4	83.45	83.25	83.35	133.22
Medium KNN	81.4	81.4	81.47	81.43	229.28
Cosine KNN	81.3	81.35	81.04	81.19	233.1
Cubic KNN	80.6	80.62	80.78	80.69	480.4
Weighted KNN	82.8	82.82	82.77	82.79	211.43
Cubic SVM	**85.7**	**85.7**	**85.75**	**85.72**	306.78

Note: Bold values indicates the best accuracy.

TABLE 3 Classification results of fine-tuned NASNet Mobile features using augmented HAM10000 dataset.

	Performance measures				
Classifiers	**Accuracy (%)**	**Sensitivity (%)**	**Precision (%)**	**F1-score (%)**	**Time (sec)**
Linear SVM	92.7	92.54	92.51	92.52	330.92
Cubic SVM	93.2	93.04	93.04	93.04	466.57
Medium Gaussian SVM	92.3	92.17	92.17	92.17	524.65
Coarse Gaussian SVM	90.5	90.3	90.51	90.40	758.96
Fine KNN	87.4	87.37	87.4	87.30	592.8
Medium KNN	87.9	87.87	87.91	87.89	596.12
Cosine KNN	87.8	87.85	87.7	87.78	587.67
Cubic KNN	87.4	87.41	87.5	87.45	600.5
Weighted KNN	88.5	88.55	88.6	88.57	476.88
Quadratic SVM	**93.2**	**93.08**	**93.05**	**93.06**	424.15

Note: Bold values indicates the best accuracy.

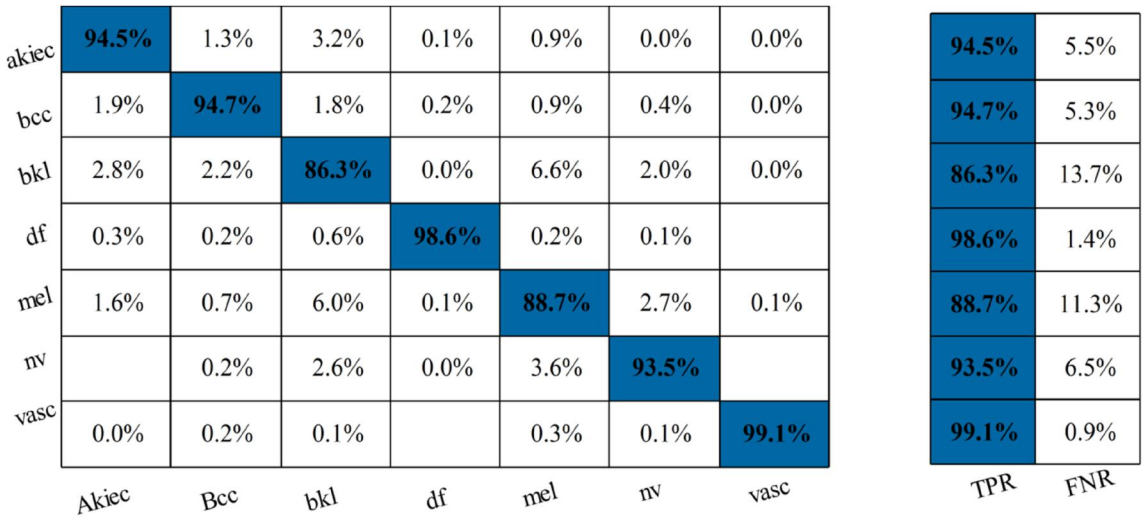

FIGURE 5 Confusion matrix of quadratic SVM for proposed fusion approach using augmented HAM10000 dataset.

TABLE 4 Classification results of the proposed framework on augmented HAM10000 dataset.

	Performance measures				
Classifiers	**Accuracy (%)**	**Sensitivity (%)**	**Precision (%)**	**F1-score (%)**	**Time (sec)**
Linear SVM	94.2	94.2	94.2	94.22	185.2
Quadratic SVM	94.4	94.3	94.4	94.3	218.8
Medium Gaussian SVM	93.9	93.8	93.9	93.9	378.6
Coarse Gaussian SVM	93.3	93.3	93.4	93.3	327.0
Fine KNN	88.5	88.57	88.55	88.5	183.3
Medium KNN	91.0	90.95	91.17	91.05	184.4
Cosine KNN	91.8	91.7	91.6	91.7	188.1
Cubic KNN	90.1	90.07	90.21	90.1	365.7
Weighted KNN	91.2	91.2	91.4	91.1	184.1
Cubic SVM	**94.4**	**94.4**	**94.4**	**94.4**	249.4

Note: Bold values indicates the best accuracy.

suggested optimisation approach. This demonstrates the power of this algorithm. Additionally, this experiment's computational time is shorter than that of the preceding three trials.

4.2 | Discussion

In this section, we summarise the overall framework's qualitative analysis results. Figure 1 depicts the proposed framework for classifying multi-class skin lesions. Initially, using the proposed hybrid approach improves the contrast. This step aims to obtain better features that will later be used to classify skin lesions with greater accuracy. Figure 7 depicts the outcomes of the middle steps. The accuracy is improved after the contrast enhancement step, as shown in this figure. The improvement in accuracy is nearly 3%–4% after using this step, demonstrating the strength of this phase. The fusion process also improves the accuracy but increases the computational time, as depicted in Figure 8. In this figure, it is clearly shown that the testing time is jumped after the fusion process. This issue is resolved through the feature selection algorithm called VcMPA. After employing this algorithm, accuracy is a little improved, but time is significantly reduced, as shown in Figure 8. Hence, this algorithm is a primary strength of the proposed framework. In addition, we performed a confidence interval-based analysis of the proposed framework's accuracy. For this purpose, we executed the last step 200 times and obtained minimum and maximum accuracy. The minimum obtained accuracy after 200 iterations are 93.5%, and the maximum is 94.4%. This shows that there is only a 0.9% change is occurred. Also, based on the confidence interval, the maximum margin of error is 93.95 ± 1.557 (±1.66%) for a confidence level of 99.9999%, $4.892\sigma_{\bar{x}}$. The margin of error for different confidence levels is illustrated in Figure 9. Hence, the overall proposed framework performed well. Figure 10 compares the proposed feature selection technique with some other existing techniques. This accuracy value plotted in the figure shows that the proposed selection technique is performed better.

Lastly, the proposed framework was compared with state-of-the-art techniques that used the HAM10000 dataset for the evaluation. Table 6 presents a comparison of the proposed framework with recent techniques. Authors in ref. [50] presented a deep learning-based technique for skin cancer classification using transfer learning. They obtained an accuracy of 90.16%, a sensitivity rate of 93.91%, a precision rate of 94.63%, and an F1 Score of 94.27%. In ref. [40], the authors presented an improved Moth Flame Optimization technique and obtained maximum accuracy of 90.67%. In ref. [41], authors presented a multi-model deep neural network-based approach to extract deep features and then selected the optimal one for skin lesion classification. Using this approach,

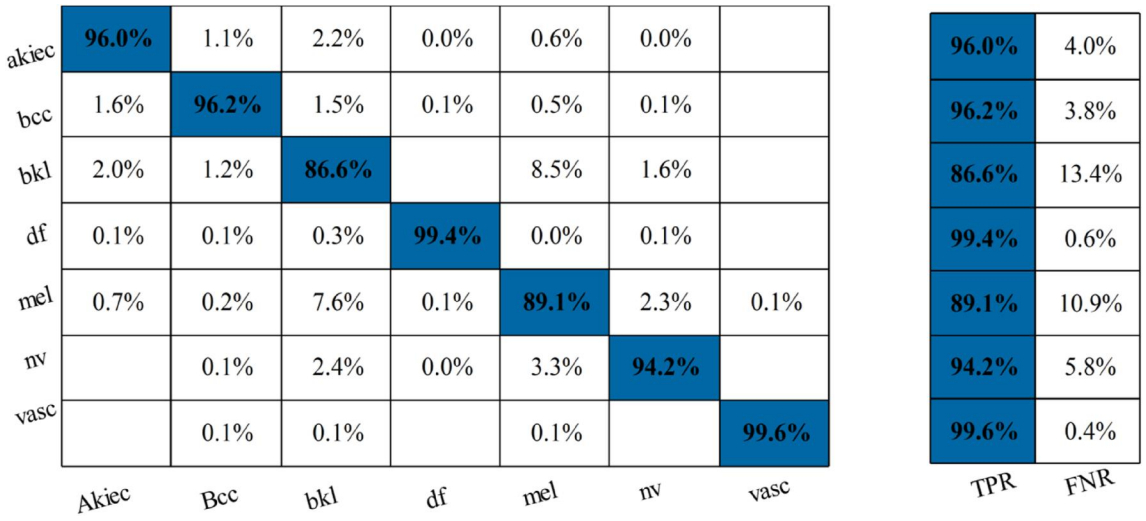

FIGURE 6 Confusion matrix of cubic SVM for proposed framework using augmented HAM10000 dataset.

TABLE 5 Classification results of proposed fusion approach on augmented HAM10000 dataset.

	Performance measures				
Classifiers	**Accuracy (%)**	**Sensitivity (%)**	**Precision (%)**	**F1-score (%)**	**Time (sec)**
Linear SVM	93.2	93.271	93.3	93.28	421.6
Cubic SVM	93.0	92.98	93.01	92.99	602.5
Medium Gaussian SVM	89.3	89.3	89.4	89.3	923.3
Coarse Gaussian SVM	89.1	89.1	89.3	89.2	801.6
Fine KNN	88.7	88.7	88.6	88.6	604.11
Medium KNN	90.8	90.8	91.05	90.92	680.2
Cosine KNN	92.1	92.17	91.07	92.11	620.3
Cubic KNN	90.0	89.98	90.22	90.09	790.5
Weighted KNN	91.9	91.12	91.32	91.21	495
Quadratic SVM	**93.6**	**93.62**	**93.68**	**93.65**	519.4

Note: Bold values indicates the best accuracy.

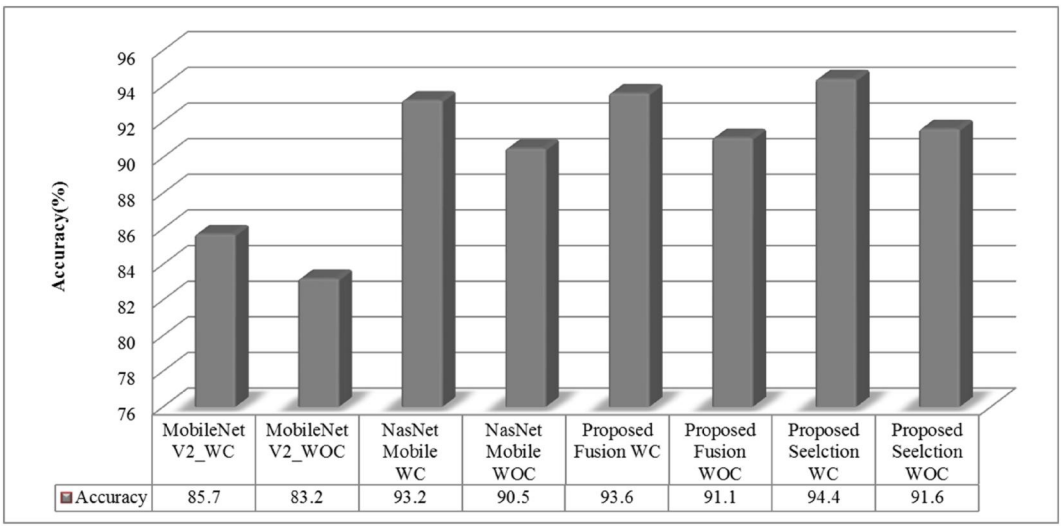

FIGURE 7 Middle steps results of proposed framework using augmented HAM10000 dataset results. *WC represents the employing contrast enhancement, and WOC represents without contrast enhancement results.

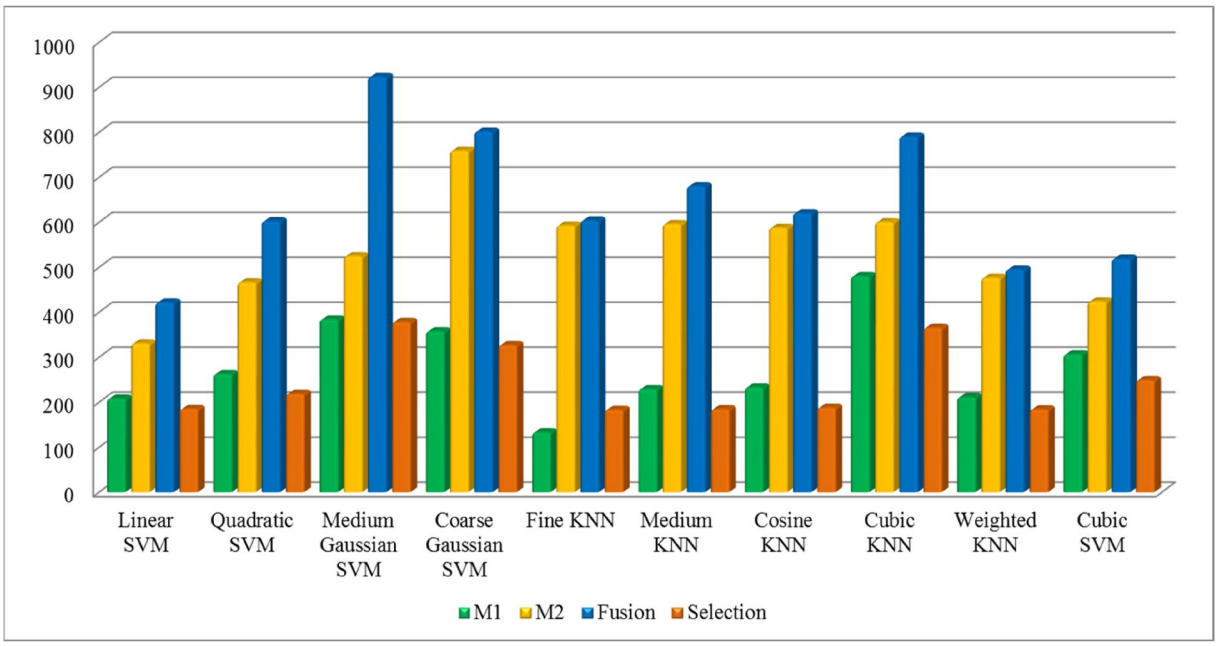

FIGURE 8 Time plot for classification efficiency of MobileNetV2, NASNet Mobile, fused, and optimised feature vectors.

Confidence Level	Margin of Error	Error Bar
68.3%, $\sigma_{\bar{x}}$	93.95 ±0.318 (±0.34%)	
90%, $1.645\sigma_{\bar{x}}$	93.95 ±0.523 (±0.56%)	
95%, $1.960\sigma_{\bar{x}}$	93.95 ±0.624 (±0.66%)	
99%, $2.576\sigma_{\bar{x}}$	93.95 ±0.82 (±0.87%)	
99.9%, $3.291\sigma_{\bar{x}}$	93.95 ±1.047 (±1.11%)	
99.99%, $3.891\sigma_{\bar{x}}$	93.95 ±1.238 (±1.32%)	
99.999%, $4.417\sigma_{\bar{x}}$	93.95 ±1.405 (±1.50%)	
99.9999%, $4.892\sigma_{\bar{x}}$	93.95 ±1.557 (±1.66%)	

FIGURE 9 Confidence interval-based analysis of proposed framework accuracy.

they obtained maximum accuracy of 89.8%. Recently in ref. [52], the authors presented a deep learning-based technique for dermoscopic skin lesion image classification and obtained an accuracy of 85.72%. In the proposed framework, we utilised the HAM10000 dataset for testing and obtained the improved accuracy of 94.4% and sensitivity rate of 94.40%.

4.3 | Lesion visualisation and prediction

The proposed framework features are visualised in this section using the GradCAM approach. First, the trained deep framework is used to visualise the information on the original dermoscopic images, as shown in Figure 11. In this figure, the light blue colour shows the strongest pixels or regions, whereas the brown region shows the weak points. Hence, it is important to correctly identify the strongest region for accurate classification. Based on Figure 11, we performed the final visual prediction regarding labelled images, as shown in Figure 12. In this figure, the prediction of the proposed framework has been illustrated, which is the strength of this work.

5 | CONCLUSION

This paper presents a multi-class system for skin lesion classification based on deep learning and feature selection. The suggested framework combines a number of different processes. To improve the visibility of the lesion site, a hybrid method is first developed for the contrast enhancement technique. This process enhances the capacity for learning of particular deep models that later extract some significant features. Deep transfer learning is used to train two pre-trained

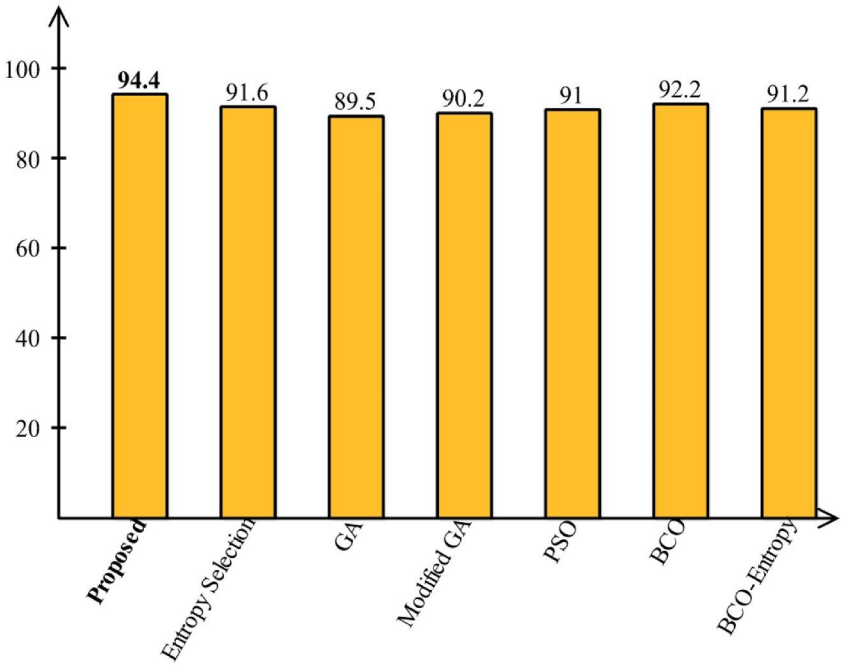

FIGURE 10 Comparison of the proposed feature selection technique with other existing techniques.

TABLE 6 Comparison of the proposed framework with state-of-the-art techniques.

References	Accuracy (%)	Sensitivity (%)	Precision (%)	F-1 score	Time (sec)
[50]	90.16	93.91	94.63	94.27	-
[40]	90.67	90.20	-	94.27	133.440
[51]	-	86	87	86	-
[41]	89.8	-	-	-	-
[52]	85.72	-	-	-	-
[53]	88.00	41.00	46.00	-	-
[54]	85.2	68.57	73.2	80.71	-
Proposed	94.4	94.4	94.4	94.4	249.4

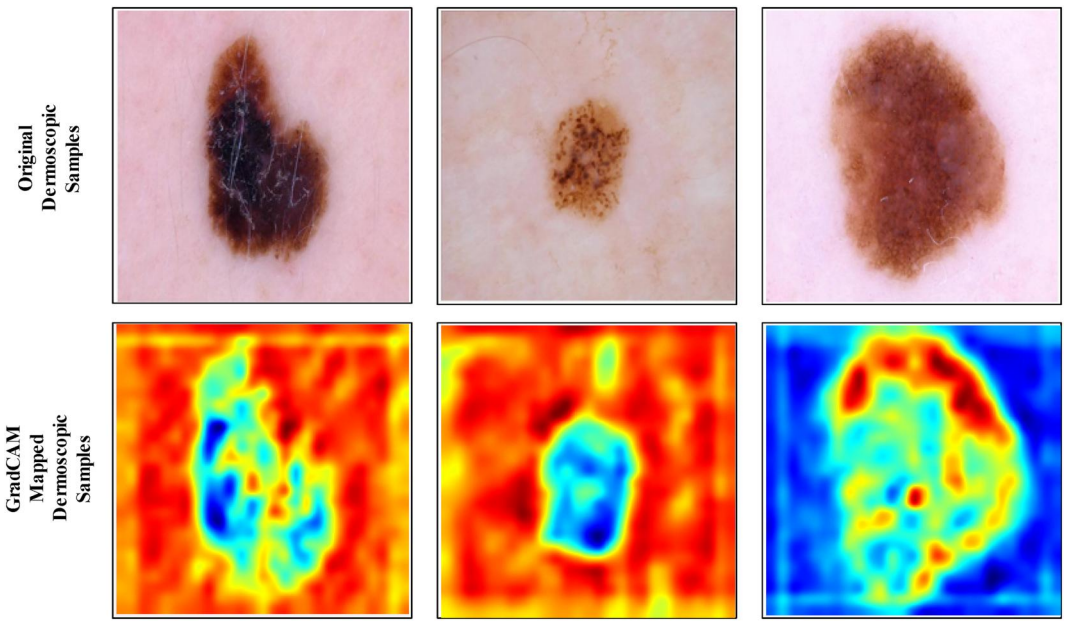

FIGURE 11 GradCAM based visualisation of the dermoscopic images using the proposed deep learning framework.

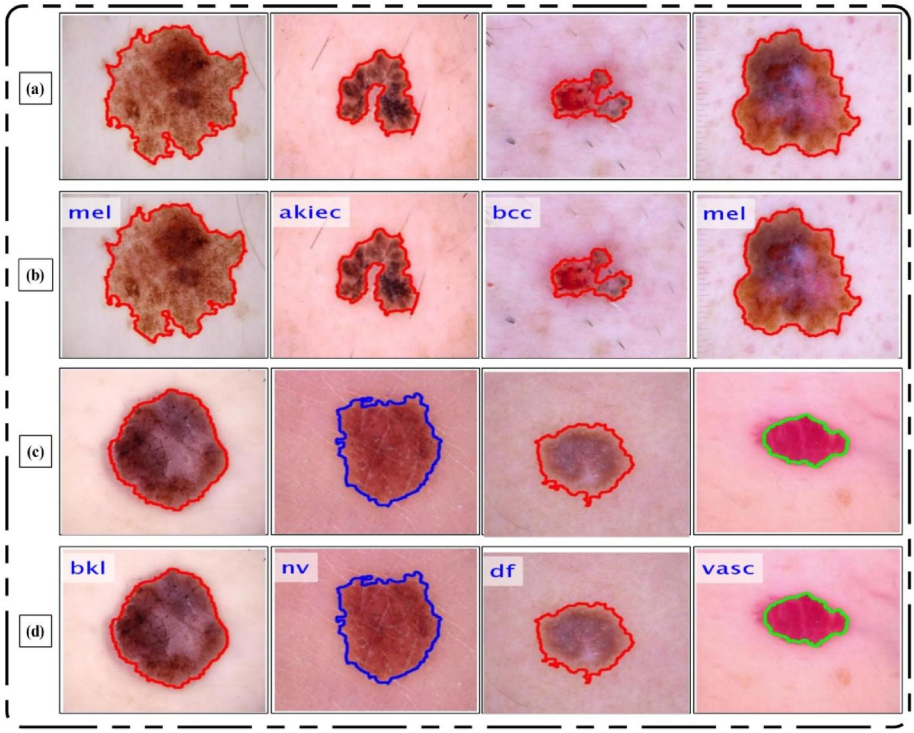

FIGURE 12 Proposed framework prediction in terms of labels on the dermoscopic images.

deep models on augmented photos. Third, using a serial-based dual threshold technique, features are taken out of the average pooling layers and combined with the data. Although the accuracy was enhanced, time jumped as a result. Through the use of the feature selection algorithm VcMPA, this problem was overcome. This algorithm shortened the computation time while increasing classification accuracy. The strength of this work is that the accuracy of the suggested framework is not affected by more than 1% after the analysis is conducted using the confidence interval. The fusion phase, which extends the computing time, is the main drawback of this study. In the future, we'll take into account an optimal fusion strategy to increase accuracy while cutting down on calculation time.

ACKNOWLEDGEMENTS

This research was funded by Princess Nourah bint Abdulrahman University Researchers Supporting Project number (PNURSP2023R333), Princess Nourah bint Abdulrahman University, Riyadh, Saudi Arabia.

CONFLICT OF INTEREST STATEMENT

The authors declare no conflict of interest.

DATA AVAILABILITY STATEMENT

Dataset used in this work is publicly available https://dataverse.harvard.edu/dataset.xhtml?persistentId=doi:10.7910/DVN/DBW86T. The source code and mat files also available here: https://drive.google.com/drive/folders/1PI0JQRpkQbhBajulEcSMo2ibGhwcNYE7?usp=sharing.

ORCID

Muhammad Attique Khan https://orcid.org/0000-0001-5723-3858
Oumaima Saidani https://orcid.org/0000-0001-9520-3174
Seifedine Kadry https://orcid.org/0000-0002-1939-4842

REFERENCES

1. Khalil, C.: Human skin explants an in vitro approach for assessing UVB induced damage. Toxicol. Vitro 53, 193–199 (2018). https://doi.org/10.1016/j.tiv.2018.08.013
2. Clinic, M.: Skin cancer. In: Book: Mayo Clinic Family Health Book, 5th ed (2023). www.mayoclinic.org/diseases-conditions/skin-cancer/symptoms-causes/syc-20377605
3. Codella, N.C., et al.: Deep learning ensembles for melanoma recognition in dermoscopy images. IBM J. Res. Dev. 61(4/5), 5.1–5.15 (2017). https://doi.org/10.1147/jrd.2017.2708299
4. Bhatia, S., Tykodi, S.S., Thompson, J.A.: Treatment of metastatic melanoma: an overview. Oncology 23, 488 (2009)
5. Kittler, H.: Evolution of the clinical, dermoscopic and pathologic diagnosis of melanoma. Dermatol. Pract. Concept. 11, 2021163S (2021). https://doi.org/10.5826/dpc.11s1a163s
6. Wang, X., et al.: Knowledge-aware deep framework for collaborative skin lesion segmentation and melanoma recognition. Pattern Recogn. 120, 108075 (2021). https://doi.org/10.1016/j.patcog.2021.108075
7. Aravind, K., et al.: Disease classification in maize crop using bag of features and multiclass support vector machine. In: 2018 2nd International Conference on Inventive Systems and Control (ICISC), pp. 1191–1196 (2018)
8. LeCun, Y., et al.: Gradient-based learning applied to document recognition. Proc. IEEE 86(11), 2278–2324 (1998). https://doi.org/10.1109/5.726791
9. Ahila Priyadharshini, R., et al.: Maize leaf disease classification using deep convolutional neural networks. Neural Comput. Appl. 31(12), 8887–8895 (2019). https://doi.org/10.1007/s00521-019-04228-3

10. Menzies, S.W., et al.: Frequency and morphologic characteristics of invasive melanomas lacking specific surface microscopic features. Arch. Dermatol. 132(10), 1178–1182 (1996). https://doi.org/10.1001/archderm.132.10.1178
11. Burada, S., Swamy, B., Kumar, M.S.: Computer-aided diagnosis mechanism for melanoma skin cancer detection using radial basis function network. In: Proceedings of the International Conference on Cognitive and Intelligent Computing, pp. 619–628 (2022)
12. Wang, S., Zhang, Y., Zhang, Y.: A blockchain-based framework for data sharing with fine-grained access control in decentralized storage systems. IEEE Access 6, 38437–38450 (2018). https://doi.org/10.1109/access.2018.2851611
13. Ahmed, A., Boopathy, P., Sudhagara Rajan, S.: Artificial intelligence for the novel corona virus (COVID-19) pandemic: opportunities, challenges, and future directions. Int. J. E Health Med. Commun. 13(2), 1–21 (2021). https://doi.org/10.4018/ijehmc.20220701.oa5
14. Yammine, K., Assi, C.: A meta-analysis of the outcomes of split-thickness skin graft on diabetic leg and foot ulcers. Int. J. Low. Extrem. Wounds 18(1), 23–30 (2019). https://doi.org/10.1177/1534734619832123
15. Gajera, H.K., Nayak, D.R., Zaveri, M.A.: A comprehensive analysis of dermoscopy images for melanoma detection via deep CNN features. Biomed. Signal Process Control 79, 104186 (2023). https://doi.org/10.1016/j.bspc.2022.104186
16. Malibari, A.A., et al.: Optimal deep neural network-driven computer aided diagnosis model for skin cancer. Comput. Electr. Eng. 103, 108318 (2022). https://doi.org/10.1016/j.compeleceng.2022.108318
17. Abayomi-Alli, O.O., et al.: Malignant skin melanoma detection using image augmentation by oversamplingin nonlinear lower-dimensional embedding manifold. Turk. J. Electr. Eng. Comput. Sci. 29(SI-1), 2600–2614 (2021). https://doi.org/10.3906/elk-2101-133
18. Khattar, S., Kaur, R.: Computer assisted diagnosis of skin cancer: a survey and future recommendations. Comput. Electr. Eng. 104, 108431 (2022). https://doi.org/10.1016/j.compeleceng.2022.108431
19. Chen, P., Huang, S., Yue, Q.: Skin lesion segmentation using recurrent attentional convolutional networks. IEEE Access 10, 94007–94018 (2022). https://doi.org/10.1109/access.2022.3204280
20. Vyas, A.H., et al.: Tear film breakup time-based dry eye disease detection using convolutional neural network. Neural Comput. Appl., 1–19 (2022). https://doi.org/10.1007/s00521-022-07652-0
21. Jain, S., Pise, N.: Computer aided melanoma skin cancer detection using image processing. Procedia Comput. Sci. 48, 735–740 (2015). https://doi.org/10.1016/j.procs.2015.04.209
22. Reddy, G.T., Khare, N.: Heart disease classification system using optimised fuzzy rule based algorithm. Int. J. Biomed. Eng. Technol. 27(3), 183–202 (2018). https://doi.org/10.1504/ijbet.2018.10015307
23. Maqsood, S., Damaševičius, R.: Multiclass skin lesion localization and classification using deep learning based features fusion and selection framework for smart healthcare. Neural Network. 160, 238–258 (2023). https://doi.org/10.1016/j.neunet.2023.01.022
24. Picon Ruiz, A., et al.: Why deep learning performs better than classical machine learning? Dyna Ingenieria E Industria 95(1), 119–122 (2020). https://doi.org/10.6036/9574
25. Stiff, K.M., et al.: Artificial intelligence and melanoma: a comprehensive review of clinical, dermoscopic, and histologic applications. Pigment Cell Melanoma Res. 35(2), 203–211 (2022). https://doi.org/10.1111/pcmr.13027
26. Bozkurt, F.: Skin lesion classification on dermatoscopic images using effective data augmentation and pre-trained deep learning approach. Multimed. Tool. Appl. 82(12), 18985–19003 (2023). https://doi.org/10.1007/s11042-022-14095-1
27. Wang, Y., et al.: Ssd-kd: a self-supervised diverse knowledge distillation method for lightweight skin lesion classification using dermoscopic images. Med. Image Anal. 84, 102693 (2023). https://doi.org/10.1016/j.media.2022.102693
28. Kareem, O.S., Abdulazee, A.M., Zeebaree, D.Q.: Skin lesions classification using deep learning techniques. Asian J. Res. Comp. Sci., 1–22 (2021). https://doi.org/10.9734/ajrcos/2021/v9i130210
29. Adegun, A., Viriri, S.: Deep learning techniques for skin lesion analysis and melanoma cancer detection: a survey of state-of-the-art. Artif. Intell. Rev. 54(2), 811–841 (2021). https://doi.org/10.1007/s10462-020-09865-y
30. Saeed, J., Zeebaree, S.: Skin lesion classification based on deep convolutional neural networks architectures. J. Appl. Sci. Technol. Trends 2(01), 41–51 (2021). https://doi.org/10.38094/jastt20189
31. Afza, F., et al.: Multiclass skin lesion classification using hybrid deep features selection and extreme learning machine. Sensors 22(3), 799 (2022). https://doi.org/10.3390/s22030799
32. Babna, K., Nair, A.T., Haritha, K.: Multi-class detection of skin disease: detection using HOG and CNN hybrid feature extraction. In: Intelligent Data Communication Technologies and Internet of Things, pp. 1025–1037. Springer (2022)
33. Iqbal I, Y.M., et al.: Automated multi-class classification of skin lesions through deep convolutional neural network with dermoscopic images. Comput. Med. Imag. Graph. 88, 101843 (2021). https://doi.org/10.1016/j.compmedimag.2020.101843
34. Khan, M.A., et al.: Developed Newton-Raphson based deep features selection framework for skin lesion recognition. Pattern Recogn. Lett. 129, 293–303 (2020). https://doi.org/10.1016/j.patrec.2019.11.034
35. Bisla, D., et al.: Skin lesion segmentation and classification with deep learning system. arXiv preprint arXiv:1902.06061, 1–6 (2019)
36. Hasan, S.N., et al.: Skin lesion segmentation by using deep learning techniques. In: 2019 Medical Technologies Congress (TIPTEKNO), pp. 1–4 (2019)
37. Khan, M.A., et al.: Construction of saliency map and hybrid set of features for efficient segmentation and classification of skin lesion. Microsc. Res. Tech. 82(6), 741–763 (2019). https://doi.org/10.1002/jemt.23220
38. Sikkandar, M.Y., et al.: Deep learning based an automated skin lesion segmentation and intelligent classification model. J. Ambient Intell. Hum. Comput. 12(3), 3245–3255 (2021). https://doi.org/10.1007/s12652-020-02537-3
39. Kumar Gondhi, N., Kumar Lehana, P.: An evolutionary approach for the enhancement of dermatological images and their classification using deep learning models. J. Healthc. Eng. 2021, 1–13 (2021). https://doi.org/10.1155/2021/8113403
40. Khan, M.A., et al.: Skin lesion segmentation and multiclass classification using deep learning features and improved moth flame optimization. Diagnostics 11(5), 811 (2021). https://doi.org/10.3390/diagnostics11050811
41. Khan, M.A., et al.: Multi-model deep neural network based features extraction and optimal selection approach for skin lesion classification. In: 2019 International Conference on Computer and Information Sciences (ICCIS), pp. 1–7 (2019)
42. Ali, R., et al.: Skin lesion segmentation and classification for ISIC 2018 by combining deep CNN and handcrafted features. arXiv preprint arXiv:1908.05730 (2019)
43. Khan, M.A., et al.: An integrated framework of skin lesion detection and recognition through saliency method and optimal deep neural network features selection. Neural Comput. Appl. 32(20), 15929–15948 (2020). https://doi.org/10.1007/s00521-019-04514-0
44. Rajinikanth, V., et al.: Skin melanoma segmentation using VGG-UNet with Adam/SGD optimizer: a study. In: 2022 Third International Conference on Intelligent Computing Instrumentation and Control Technologies (ICICICT), pp. 982–986 (2022)
45. Mohammed, M.A., et al.: A hybrid cancer prediction based on multi-omics data and reinforcement learning state action reward state action (SARSA). Comput. Biol. Med. 154, 106617 (2023). https://doi.org/10.1016/j.compbiomed.2023.106617
46. Alenezi, F., Armghan, A., Polat, K.: Wavelet transform based deep residual neural network and ReLU based Extreme Learning Machine for skin lesion classification. Expert Syst. Appl. 213, 119064 (2023). https://doi.org/10.1016/j.eswa.2022.119064
47. Tschandl, P., Rosendahl, C., Kittler, H.: The HAM10000 dataset, a large collection of multi-source dermatoscopic images of common pigmented skin lesions. Sci. Data 5, 1–9 (2018). https://doi.org/10.1038/sdata.2018.161

48. Sandler, M., et al.: Mobilenetv2: inverted residuals and linear bottlenecks. In: Proceedings of the IEEE Conference on Computer Vision and Pattern Recognition, pp. 4510–4520 (2018)
49. Zoph, B., et al.: Learning transferable architectures for scalable image recognition. In: Proceedings of the IEEE Conference on Computer Vision and Pattern Recognition, pp. 8697–8710 (2018)
50. Ali, M.S., et al.: An enhanced technique of skin cancer classification using deep convolutional neural network with transfer learning models. Mach. Lear. Appl. 5, 100036 (2021). https://doi.org/10.1016/j.mlwa.2021.100036
51. Bhosale, S.: Comparison of deep learning and machine learning models and frameworks for skin lesion classification. arXiv preprint arXiv:2207.12715 (2022)
52. Patel, M.B.: Multi class skin diseases classification based on dermoscopic skin images using deep learning. Int. J. Next-Gener. Comput. 13 (2022). https://doi.org/10.47164/ijngc.v13i2.480
53. Camacho-Gutiérrez, J.A., Solorza-Calderón, S., Álvarez-Borrego, J.: Multi-class skin lesion classification using prism-and segmentation-based fractal signatures. Expert Syst. Appl. 197, 116671 (2022). https://doi.org/10.1016/j.eswa.2022.116671
54. Elyasi, N., Hosseini Moghadam, M.: Classification of skin lesions by Tda alongside xception neural network. J AI and Data Mining (2022)

How to cite this article: Dillshad, V., et al.: D2LFS2Net: multi-class skin lesion diagnosis using deep learning and variance-controlled Marine Predator optimisation: an application for precision medicine. CAAI Trans. Intell. Technol. 1–16 (2023). https://doi.org/10.1049/cit2.12267